Analysis of pulmonary pure ground-glass nodule in enhanced dual energy CT imaging for predicting invasive adenocarcinoma: comparing with conventional thin-section CT imaging

Ying Zhang[1]*, Jian Tang[2]*, Jianrong Xu[1], Jiejun Cheng[1], Huawei Wu[1]

[1]Department of Radiology, [2]Department of Thoracic Surgery, Renji Hospital, School of Medicine, Shanghai Jiaotong University, Shanghai 200127, China

Contributions: (I) Conception and design: All authors; (II) Administrative support: H Wu, J Cheng; (III) Provision of study materials or patients: All authors; (IV) Collection and assembly of data: All authors; (V) Data analysis and interpretation: All authors; (VI) Manuscript writing: All authors; (VII) Final approval of manuscript: All authors.

*These authors contributed equally to this work.

Correspondence to: Huawei Wu, MD; Jiejun Cheng, MD. Department of Radiology, Renji Hospital, School of Medicine, Shanghai Jiaotong University, No.160 Pujian Road, Shanghai 200127, China. Email: chest_RJ@163.com; drchjj@163.com.

Background: To investigate the value of dual energy computed tomography (DECT) parameters (including iodine concentration and monochromatic CT numbers) for predicting pure ground-glass nodules (pGGNs) of invasive adenocarcinoma (IA).

Methods: A total of 55 resected pGGNs evaluated with both unenhanced thin-section CT (TSCT) and enhanced DECT scans were included. Correlations between histopathology [adenocarcinoma in situ (AIS), minimally IA (MIA), and IA] and CT scan characteristics were examined. CT scan and clinicodemographic data were investigated by univariate and multivariate analysis to identify features that helped distinguish IA from AIS or MIA.

Results: Both normalized iodine concentration (NIC) of IA and slope of spectral curve [slope(k)] were not significantly different between IA and AIS or MIA. Size, performance of pleural retraction and enhanced monochromatic CT attenuation values of 120–140 keV were significantly higher for IA. In multivariate regression analysis, size and enhanced monochromatic CT number of 140 keV were independent predictors for IA. Using the two parameters together, the diagnostic capacity of IA could be improved from 0.697 or 0.635 to 0.713.

Conclusions: DECT could help demonstrate blood supply and indicate invasion extent of pGGNs, and monochromatic CT number of higher energy (especially 140 keV) would be better for diagnosing IA than lower energies. Together with size of pGGNs, the diagnostic capacity of IA could be better.

Keywords: Computed tomography (CT); dual energy; ground-glass opacity; lung adenocarcinoma; contrast enhanced

Introduction

In the new multidisciplinary classification on lung adenocarcinoma proposed in 2011 (1) and adopted by WHO in 2015 (2), adenocarcinoma is classified into preinvasive adenocarcinoma [atypical adenomatous hyperplasia (AAH), and adenocarcinoma in situ (AIS)], minimally invasive adenocarcinoma (MIA), and invasive adenocarcinoma (IA). The complete resection of AAH, AIS and MIA results in 100% disease-specific survival (1), while for IA, the 5-year overall survival is about 49–84% (3).

4968

Zhang et al. Contrast enhancement of pulmonary GGNs

Several researches have used thin-section CT (TSCT) to distinguish IA from the preinvasive adenocarcinoma or MIA in terms of CT number and morphologic characteristics such as size, margin, bubble lucency, and solid proportion, and have indicated that the solid proportion has correlation with the degree of invasion of ground-glass nodules (GGNs) (4-9).

Sometimes, GGNs would have no solid component, which are named pure GGNs (pGGNs). Most pGGNs tend to be preinvasive (1), while approximately 20–40% of pGGNs are pathologically malignant (10). Because of the limited resolution (0.2–0.3 mm) of CT images, stromal or myofibroblastic invasion of 5 mm or smaller in MIA or even IA greater than 5 mm in size may manifest as pGGN on high resolution CT (5). It has been proved that CT attenuation of IA is higher than its precursors (11), but there is no consensus over the cutoff of CT attenuation to indicate pGGN of IA. One study suggests that pGGNs with mean CT attenuation >–472 Hounsfield unit (HU) are more likely to be IA, with sensitivity of 75% and specificity of 81% (12). Angiogenesis is a fundamental process in the development of tumors, but enhancement characteristics of GGNs are often very difficult to assess because of low cellularity, and there are few researches about the enhancement characteristics of GGNs. Li *et al.* (13) found that the solid proportion of some GGNs (mostly in MIA or IA) would increase after contrast enhancement, and it could help for diagnosis of GGNs.

Gemstone spectral imaging (GSI) analysis software is a specific tool in dual energy computed tomography (DECT) with the fast-kVp-switching mode, and it provides material density measurement using the material decomposition images and generates CT attenuation value as function of photon energy using the 101 sets of virtual monochromatic images generated in the dual energy spectral CT imaging (14). Using iodine decomposition imaging of DECT, some researchers have observed enhancement of GGNs (14-16). Because iodine concentration (IC) would not be affected by air in lesions, it is considered to reflect blood volume better than CT number in GGNs (14). Additionally, DECT can also provide information about the attenuation changes in different materials as a function of X-ray photon energy (17,18). The energy-dependent attenuation information has not been fully explored in assessing GGNs, and we hypothesized that the information regarding these CT attenuation values might help the differentiation of pGGNs.

Thus, the purpose of our study was to investigate the value of using DECT parameters (including IC and CT numbers in monochromatic images) for distinguishing IA from AIS or MIA.

Methods

This research was approved by Institutional Ethics Board of Renji Hospital, School of Medicine, Shanghai Jiaotong University (No. 2017-082). Written informed consent for the use of CT scanning information was obtained from each patient.

Subjects

We retrospectively reviewed our patient database between July 2015 and December 2016 to identify patients with GGNs who underwent contrast-enhanced DECT scans. The inclusion criteria were: (I) pathologically confirmed; (II) diameters between 8 and 30 mm, GGNs <8 mm were excluded because pGGNs of <8 mm may rarely represent IA; (III) composed of pGGNs on lung window images (window width, 1,500 HU; window level, –600 HU) that had no identifiable soft-tissue attenuation within the lesion on the mediastinal window images (window width, 400 HU; window level, 20 HU). We did not regard blood vessels as solid components despite their solid appearance.

Based on these criteria, 58 pGGNs in 56 patients were included. Of the 56 patients, two patients had two pGGNs (≥8 mm) in different lobes, and three patients with other GGNs in different lobes or lungs were excluded for reasons of having solid component (n=1) or <8 mm (n=2).

CT examinations

All patients underwent CT examinations on a Discovery CT750HD scanner (GE Healthcare, WI). The non-enhanced scan was performed first with the conventional helical mode at a tube voltage of 120 kVp; tube current, 180 mA; helical pitch, 1.375; slice thickness and interval, 1.25 mm/1.25 mm. For the contrast-enhanced CT scan, 80–100 mL (1.35 mL/kg of body weight) nonionic iodinated contrast material (iopamidol, 370 mg/mL; Shanghai Bracco Sine Pharmaceutical Co. Ltd., China) was administrated at a rate of 3.0 mL/s by using a power injector (OptiVantage, tyco Healthcare, Cincinnati), and the enhancement scan delay time was 85 s after the beginning of injection. The contrast-enhanced scan was carried out with the dual energy spectral CT mode with fast tube voltage switching between 80 and 140 kVp on adjacent views during a single rotation. The other DECT parameters were the following: tube rotation time, 0.6 s; tube current, 275 mA; helical pitch, 1.375; field of view, 500 mm; slice thickness and interval,
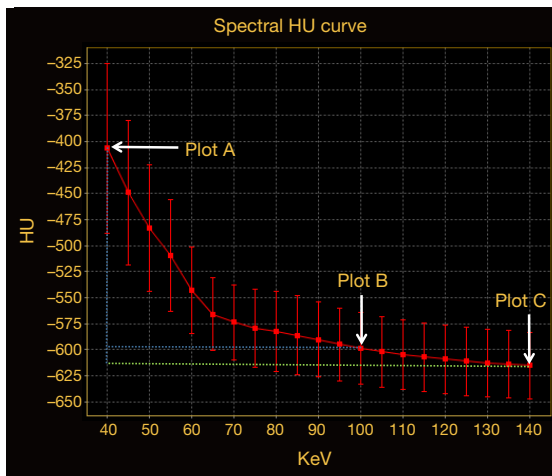
Figure 1 Spectral HU curve of a pGGN confirmed to be invasive adenocarcinoma. Plots A-C were respectively the value of CT attenuation of 40, 100, 140 keV monochromatic image. The slope between plots A and B was sharp, while almost flat between plots B and C. HU, Hounsfield unit; pGGN, pure ground-glass nodule.

1.25 mm/1.25 mm. Two types of images were obtained from the reconstruction of DECT imaging automatically with GSI viewer software (GE Healthcare) for each patient using adaptive statistical iterative reconstruction (ASIR) method: the iodine-based material decomposition images and a set of monochromatic images at energies ranging from 40 to 140 keV.

Data analysis

Three radiologists (H Wu, J Cheng and Y Zhang with 15, 18 and 7 years of experience in chest CT, respectively) unaware of patient information and pathologic results interpreted the images and measured the quantitative parameters on an advanced workstation (ADW4.4; GE Healthcare) independent of each other, and their disagreement on measurement was resolved by consensus.

Size measurement and morphological evaluations

Lesion attenuation and maximum diameter were measured on the multiple planar reformat (MPR) unenhanced images with a lung window setting (WW, 1500 HU; WL, –600 HU). For attenuation measurement, a region of interest (ROI) covering the largest possible area of each nodule was drawn on the slice showing the maximum diameter of unenhanced imaging. Pulmonary vessels and bronchi were excluded from the ROIs.

In terms of morphological characteristics, the presence of bubble lucency, lobulated border and pleural retraction were documented and evaluated. Bubble lucency was defined as small spots of air attenuation within lesions. Lobulated border was defined when a portion of a lesion's surface showed a wavy or scalloped configuration, excepting regions abutting the pleura. Pleural retraction was defined as retraction of the pleura toward the lesion. Vessels characteristics in pGGNs were classified into four types: type I, the vessels circumventing GGN; type II, the vessels going through GGN without any morphological changes; type III, the vessels distorted or being rigid but without increase in amount or converge toward the lesion; type IV, the vessels going through GGN with broadened lumen or gathered appearances. Bronchi characteristics in pGGNs were classified into three types: type I, the bronchi distorted and extent in the GGN; type II, the bronchi going through GGN without any morphological changes; type III, the bronchi circumventing GGN.

Quantitative measurements on enhanced DECT images

On the enhanced spectral imaging, CT number, IC of lesions were respectively measured from the monochromatic 40–140 keV images at a 10-keV interval, and iodine-based material decomposition images. Pulmonary artery and bronchi were avoided when ROI was drawn. To minimize variations caused by the patient's circulation status, a circular ROI was put in the thoracic aorta at the same slice of imaging with the ROI of pGGN, and the IC value of pGGN was normalized to that of thoracic aorta to derive the normalized IC (NIC): IC_{pGGN}/IC_{aorta}. For the CT number measurement, the GSI software also automatically propagated the ROIs to all the monochromatic image sets with energies from 40 to 140 keV to generate the spectral attenuation curves. The slope of such curve [slope(k)] was calculated as the CT attenuation difference at two energy levels (40 and 100 keV) divided by the energy difference (60 keV) from the spectral curve: slope(k) = |monochromatic CT number of 40 keV – monochromatic CT number of 100 keV|/60. As in general, the curve between 100 and 140 keV was almost flat, we chose the range of 40 and 100 keV of which the slope was larger to improve the sensitivity of describing different slope(k) than the whole range (*Figure 1*).

Statistical analysis

Commercial statistical analysis packages (version 22.0.0 SPSS,

4970

Zhang et al. Contrast enhancement of pulmonary GGNs

Table 1 Characteristics of patients or pGGNs

Characteristics	Values
Sex, n (%)	
Male	13 (24.5)
Female	40 (75.5)
Age, range [median] (years)	27–82 [59]
Smoking habits, n (%)	
Nonsmoker	53 (100.0)
Current/former smoker	0 (0)
Histologic types, n (%)	
AIS	21 (38.2)
MIA	19 (34.5)
IA	15 (27.3)
Surgical procedure, n (%)	
Lobectomy	22 (40.0)
Sublobar resection	33 (60.0)
Pathologic T stage, n (%)	
Tis	21 (38.2)
T1a	12 (21.8)
T1b	16 (29.1)
T1c	6 (10.9)

pGGN, pure ground-glass nodule; AIS, adenocarcinoma in situ; IA, invasive adenocarcinoma; MIA, minimally IA.

IBM) were used to analyze the measurements. A P value <0.05 was considered as statistically significant. For the evaluation of interobserver agreement, intraclass correlation coefficients (ICCs) were calculated for the quantitative parameters and k index for morphologic characteristics.

Because AIS and MIA had similar prognoses, these two subtypes of pGGNs were combined into a single group and compared with the IA. The two groups were compared using either Student's *t*-test (all quantitative CT parameters) or the Kruskal-Wallis test (age, size) for continuous variables, and using the Fisher's exact test for categorical variables (sex, the presence of bubble lucency, lobulation, and pleural retraction, bronchi or vessels characteristics). Correlations between histopathologic diagnoses and the CT scan characteristics were performed to investigate which CT scan findings were predictive of IA using Spearman rank correlation test.

Univariate analysis was conducted to identify factors related to the stratification of IA *vs.* AIS or MIA on the

basis of test results (P<0.05). For multivariate analysis, logistic regression analysis was used with multicollinearity examination by using the Spearman rank correlation test. Receiver operating characteristic (ROC) curve analysis was performed to determine the cutoff value, the sensitivity, specificity and accuracy of the significant predictive factor.

Results

Patients

Within the 58 pGGNs, there were only three cases of AAH. As AAH are usually smaller than the other histological types of adenocarcinoma (5), and to reduce the extent of unbalance among different histological types of adenocarcinoma, the three cases of AAH were removed. At last, 55 pGGNs in 53 patients were included. The study population was 13 men (median age, 61 years; range, 32–75 years) and 40 women (median age, 56.5 years; range, 27–82 years). The clinicopathologic characteristics of the 53 patients are summarized in *Table 1*. The mean size of the 55 pGGNs was 14.2 mm (standard deviation, ±6.0 mm; range, 8.0–27.0 mm). All patients were nonsmokers. None of the patients had enlarged lymph nodes (>10 mm in short-axis diameter) on CT scans. Among the 55 pGGNs, 21 were AIS, 19 were MIA, and 15 were IA. Both age (P=0.248) and gender (P=0.244) of patients between IA and AIS or MIA did not differ significantly.

Inter-observer agreement

Interobserver agreement for measurements is shown in *Table 2*. The ICCs for quantitative parameters were very high, whereas those for morphologic features were medium to high.

Morphological characteristics of pGGNs

Morphological features of the 55 pGGNs corresponding to the IA and AIS or MIA are recorded in *Table 3*. Presence of bubble lucency was rarely observed in pGGNs, with limited diagnostic capacity of IA (adjusted P=0.475 IA *vs.* AIS or MIA). Pleural retraction and lobulation were both more frequent in IA than in AIS or MIA, and the difference between the two groups was significant for the presence of pleural retraction (adjusted P=0.020), while not significant for presence of lobulation (adjusted P=0.727) (*Figures 2-4*). Bronchi circumvented most pGGNs (type III), then following with type II in AIS, while type I in MIA

Table 2 Interobserver agreement for assessing CT scan features

Variates	ICCs	k index
Size	0.980	–
Non-enhanced CT number	0.973	–
Enhanced monochromatic CT number		
40 keV	0.908	–
50 keV	0.903	–
60 keV	0.899	–
70 keV	0.895	–
80 keV	0.891	–
90 keV	0.890	–
100 keV	0.888	–
110 keV	0.887	–
120 keV	0.887	–
130 keV	0.886	–
140 keV	0.886	–
NIC	0.938	–
Slope(k)	0.887	–
Bubble lucency	–	0.650*/0.650[#]/0.481[^]
Lobulation	–	0.658*/1.000[#]/0.658[^]
Pleura retraction	–	0.741*/0.692[#]/0.566[^]
Bronchi in pGGNs	–	0.747*/0.625[#]/0.605[^]
Vessels in pGGNs	–	0.719*/0.548[#]/0.704[^]

*, comparison between observer 1 and 2; [#], comparison between observer 1 and 3; [^], comparison between observer 2 and 3. ICC, intraclass correlation coefficient; CT, computed tomography; NIC, normalized iodine concentration; slope(k), slope of spectral curve; pGGN, pure ground-glass nodule.

and IA. And the difference of characteristics of bronchi was not significant between IA and AIS or MIA (P=0.255). The vessels were mostly observed going through pGGN without any morphological changes (type II) in AIS, while going through GGN with broadened lumen or a gathered appearance of vessels (type IV) in MIA (*Figure 3*) or IA (*Figure 4*). And the difference of characteristics of vessels was not significant between IA and AIS or MIA (P=0.516).

Quantitative characteristics of pGGNs

Quantitative characteristics of the 55 pGGNs corresponding to IA and AIS or MIA are recorded in *Table 4*. The size of IA group was significantly larger than AIS or MIA (P=0.026).

In the non-enhanced TSCT imaging, CT attenuation of AIS or MIA was lower than that of IA, but the difference was not significant (t=−1.790, P=0.079) (*Table 4*). The same results were observed for comparing the two groups for enhanced monochromatic CT attenuation with energy from 40–110 keV (*Table 4*) (P=0.050–0.276), while for energies between 120–140 keV, significant differences were recognized (P=0.044–0.048) (*Table 4*).

For the iodine-based images in enhanced DECT, the NIC of IA group was slightly higher than AIS or MIA without significant difference (t=0.487, P=0.629). Besides, there was no significant difference for slope(k) between the two groups (t=1.010, P=0.317) (*Table 4*).

Correlation between imaging parameters and pathology

Relationships between all parameters and extent of invasion on pathology are shown in *Table 5*. Only size of lesions and presence of pleural retraction correlated significantly with the extent of invasion. Although enhanced monochromatic CT number of 140 keV showed no significant correlation with extent of invasion, after changing it into a binary variable as indicator of 140 keV according to the threshold acquired form ROC analysis (<−476.4 or ≥−476.4 HU), significant correlation was seen between indicator of 140 keV and the extent of invasion (r=0.298, P=0.027).

Diagnostic performances

In the univariate analysis, the presence of pleural retraction [odds ratio (OR) =4.958, P=0.019], size of lesions (OR =6.889, P=0.004) and indicator of 140 keV (OR =4.125, P=0.033) were significant factors indicating IA. In the multivariate analysis, because there was a close correlation between the presence of pleural retraction and the indicator of 140 keV (r =0.363, P=0.007), two models of analysis were performed, one with size and indicator of 140 keV (model 1), another with size and presence of pleural retraction (model 2). In model 1, both size (OR =6.383, P=0.010) and indicator of 140 keV (OR =4.774, P=0.040) favored the diagnosis of IA. And in model 2, only size favored the diagnosis of IA (OR =5.541, P=0.015). ROC curve analysis showed that the size performed well in the differentiation of IA and AIS or MIA [area under the curve (AUC) =0.697, sensitivity =66.7%, specificity =77.5%, accuracy =74.5%, threshold =16.1 mm], better than that of the enhanced monochromatic

4972

Zhang et al. Contrast enhancement of pulmonary GGNs

Table 3 The morphological characteristics of the 55 pGGNs classified into IA vs. AIS or MIA

Characteristics	AIS or MIA (n=40), n (%)	AIS (n=21), n (%)	MIA (n=19), n (%)	IA (n=15), n (%)	P values*
Bubble lucency	1 (2.5)	1 (4.8)	0 (0)	1 (6.7)	0.475
Lobulation	39 (97.5)	21 (100.0)	18 (94.7)	15 (100.0)	0.727
Pleural retraction	6 (15.0)	2 (9.5)	4 (21.1)	7 (46.7)	0.020
Bronchi in pGGNs					0.255
Type I	8 (20.0)	2 (9.5)	6 (31.6)	6 (40.0)	
Type II	7 (17.5)	4 (19.0)	3 (15.8)	3 (20.0)	
Type III	25 (62.5)	15 (71.4)	10 (52.6)	6 (40.0)	
Vessels in pGGNs					0.516
Type I	2 (5.0)	2 (9.5)	0 (0)	0 (0)	
Type II	17 (42.5)	11 (52.4)	6 (31.6)	3 (20.0)	
Type III	5 (12.5)	2 (9.5)	3 (15.8)	2 (13.3)	
Type IV	16 (40.0)	6 (28.6)	10 (52.6)	10 (66.7)	

*, P values for comparison between IA and AIS or MIA. IA, invasive adenocarcinoma; MIA, minimally IA; AIS, adenocarcinoma in situ; pGGN, pure ground-glass nodule.

CT number of 140 keV (AUC =0.635, sensitivity =46.7%, specificity =87.5%, accuracy =72.7%, threshold =–476.4 HU) in a small extent (*Figure 5*). When the two parameters were considered together for diagnosing IA, AUC increased to 0.713, with sensitivity of 80.0%, specificity of 62.5% and accuracy of 67.6%.

Discussion

Measuring the enhancement degree of pulmonary tumor which is directly related to the vascularity and distribution of the intravascular and extracellular spaces, has proven to be helpful in distinguishing malignity from benignity in dynamic contrast-enhanced CT, due to the distinct differences in the vascularity and vasculature of benign and malignant pulmonary tumors (19-20). Our previous study (21) has found that IC form iodine decomposition images has better performances in differentiating benign and malignant solid lung tumors than the net enhanced CT number. However, there are few previous researches assessing the amount of enhancement in pGGNs (14-16). Recently, Son *et al.* (16) found that combining with texture analysis and DECT imaging, the heterogeneity within the tumors on the iodine-enhanced imaging was more obvious than virtual non-contrast (VNC) imaging, and could improve the power of diagnosing IA. However, texture analysis is a complicated and time-consuming

analysis method, and is still not in common use now. And for determining IA, the average value of IC and slope(k) of pGGNs which indicating the general degree of enhancement in pGGNs, have not been reported.

In our study, the mean value of IC or slope(k) in pGGNs were similar with or even higher than the value of solid tumors (malignant, 0.55±0.23, 2.53±1.02; benign, 0.23±0.20, 1.38±1.06) in previous study (21). Since we had carefully avoided pulmonary vessels in ROIs, we considered that the degree of enhancement of pGGNs could be assessed by IC and slope(k). However, both NIC and slope(k) could not differentiate IA and AIS or MIA statistically. For the enhanced monochromatic CT number, significant difference between IA and AIS or MIA was observed only with energy between 120–140 keV. As known, iodine has markedly increased attenuation at lower energies (22). So, CT number of lower energies, especially 40–60 keV, was influenced by iodine after contrast enhancement, while CT number of 120–140 keV was less influenced by iodine. Thus, we considered that although heterogeneity of iodine distribution after contrast-enhancement in GGNs of IA was more obvious than AIS or MIA (16), the average contrast-enhancement degree of pGGN was not significantly high enough to distinct IA from AIS or MIA. This might be related to the possibly similar vessels distribution between different histological subtypes of adenocarcinoma, and further investigation
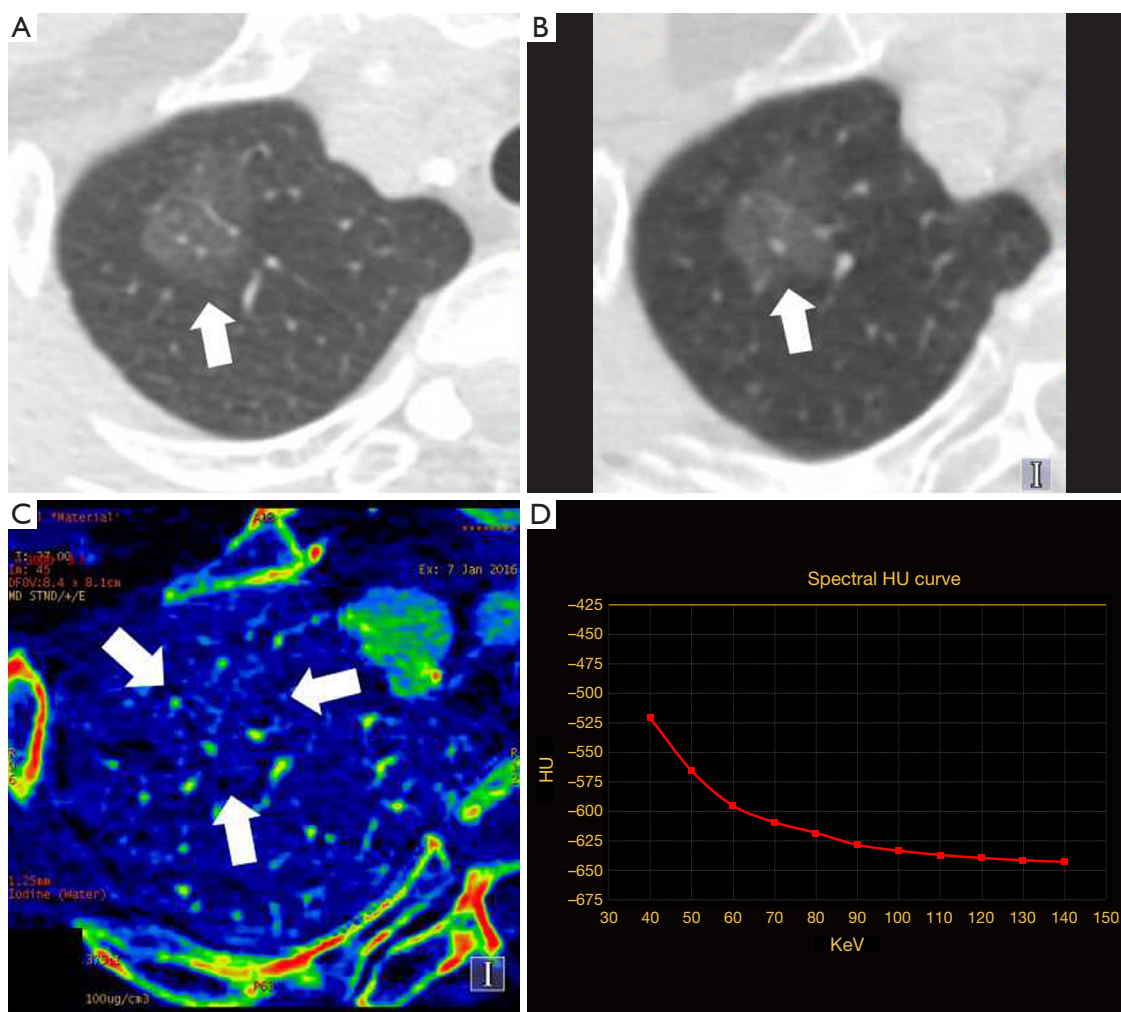
Figure 2 Adenocarcinoma in situ (AIS) in a 58-year-old woman, with maximum diameter of 26.1 mm. (A) Nonenhanced TSCT image showed presence of lobulation and normal-shaped vessels going through the pGGN in upper lobe of right lung, without pleura retraction (white arrow). The average CT attenuation value was −666.0 HU; (B) 140-keV monochromatic image after contrast enhancement (white arrow). The average CT attenuation value was −604.4 HU; (C) iodine decomposition image (the three white arrows showing the contour of the lesion). Normalized iodine concentration (NIC) was 0.28; (D) spectral curve. Slope(k) was 1.93. TSCT, thin-section computed tomography; pGGN, pure ground-glass nodule; HU, Hounsfield unit; slope(k), slope of spectral curve.

about quantifying microvessel densities which may help to explain it is needed.

Similar to the former studies (5,10,12), the nonenhanced CT number of IA was higher than that of AIS or MIA, but the difference was not obvious in our study, and this result did not concur with the former researches (5,10,12). The possible reason could be the small number of cases of IA, however, enhanced monochromatic CT number of 120–140 keV which was less influenced by iodine, performed better than nonenhanced CT number to indicate IA. Because polychromatic X-ray beams would be affected by the beam hardening effect, while truly monochromatic X-ray beams do not (22), the monochromatic CT number would be more accurate than polychromatic CT number. However, as the purpose of our study was to evaluate the enhancement characteristics of pGGNs, nonenhanced monochromatic CT number was not included. The further research to discover the diagnostic capacity of IA using the CT number in nonenhanced monochromatic image would be needed in the future.

In previous study, it has been proved that pGGN with size >8 mm was an important predictor of malignancy (10)
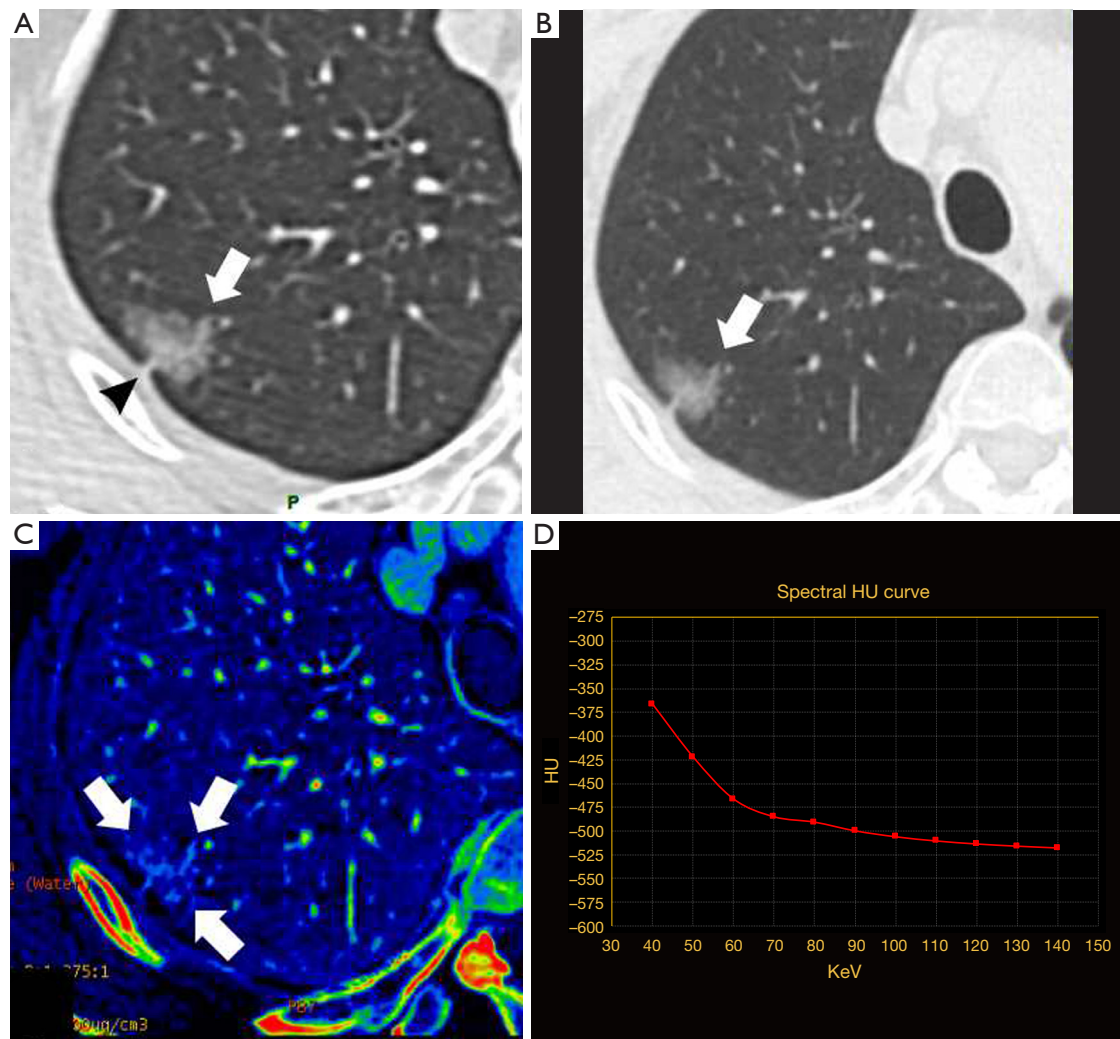
4974

Zhang et al. Contrast enhancement of pulmonary GGNs

Figure 3 Minimally invasive adenocarcinoma (MIA) in a 64-year-old woman, with maximum diameter of 15.6 mm. (A) Nonenhanced TSCT image showed a pGGN with broadened vessels going through it, presence of lobulation (white arrow) and pleura retraction (black arrow head) in upper lobe of right lung. The average CT attenuation value was –403.0 HU; (B) 140-keV monochromatic image after contrast enhancement (white arrow). The average CT attenuation value was –416.4 HU; (C) iodine decomposition image (the three white arrows showing the contour of the lesion). Normalized iodine concentration (NIC) was 0.59; (D) spectral curve. Slope(k) was 3.14. TSCT, thin-section computed tomography; pGGN, pure ground-glass nodule; HU, Hounsfield unit; slope(k), slope of spectral curve.

and pGGNs with diameter greater than 15 mm are more likely to be IA (11). In our study, the maximum diameter greater than 16.1 mm indicated IA independently, and this was similar with previous study (5-8,23,24). And when using a threshold of greater or equal to16.1 mm for size measurement and enhanced monochromatic CT number of 140 keV greater or equal to –476.4 HU together, the diagnostic capacity and sensitivity for IA increased. This means that size and CT number in enhanced

monochromatic image at 140 keV were complementary parameters for the diagnosis of IA.

Regarding the morphologic CT features of pGGNs, in previous study, an internal air bronchogram (5,8,24) or pleural retraction (6,7) are associated with invasiveness of GGNs or even pGGNs (5-8). While another study (25) reported that no significant morphologic differences were observed in pGGNs, including bubble lucency, lobulation, spiculation and pleural retraction. In our study, there was
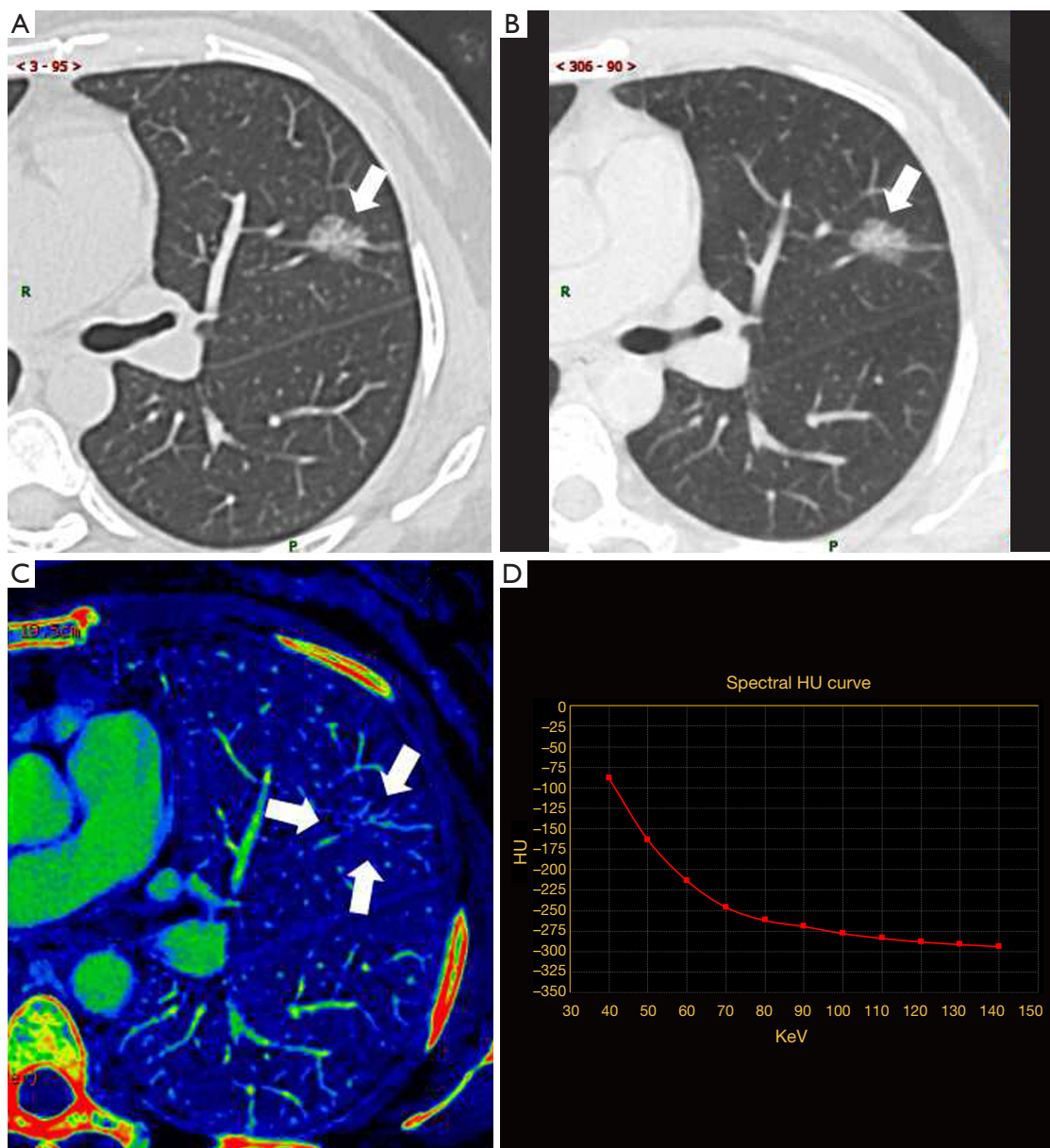
Figure 4 Invasive adenocarcinoma (IA) in a 48-year-old woman, with maximum diameter of 17.1 mm. (A) Nonenhanced TSCT image showed a pGGN in upper lobe of left lung, with presence of lobulation and vessels going through it with broadened lumen and gathered appearance (white arrow). The average CT attenuation value was –323.0 HU; (B) 140-keV monochromatic image after contrast enhancement (white arrow). The average CT attenuation value was –295.6 HU; (C) iodine decomposition image (the three white arrows showing the contour of the lesion). Normalized iodine concentration (NIC) was 0.46; (D) spectral curve. Slope(k) was 2.83. TSCT, thin-section computed tomography; pGGN, pure ground-glass nodule; HU, Hounsfield unit; slope(k), slope of spectral curve.

Table 4 Quantitative characteristics of the 55 pGGNs classified into IA vs. AIS or MIA

Parameters	AIS or MIA (n=40)	AIS (n=21)	MIA (n=23)	IA (n=15)	P values*
Size [mean ± SD (min–max)] (mm)	13.2±5.7 (8.0–27.0)	13.6±6.9 (8.0–27.0)	12.8±4.1 (8.5–22.3)	17.1±6.2 (9.1–25.8)	0.026
Unenhanced TSCT imaging (mean ± SD) (HU)					
CT number	−545.9±115.0	−562.7±131.2	−527.4±94.1	−476.5±159.1	0.079
GSI contrast-enhanced imaging (mean ± SD)					
CT number of monochromatic imaging (HU)					
40 keV	−378.4±139.9	−394.5±169.4	−360.6±99.6	−327.8±180.9	0.276
50 keV	−445.7±123.2	−465.7±147.4	−423.7±88.0	−387.8±164.5	0.163
60 keV	−496.6±111.8	−519.4±131.2	−471.3±81.8	−430.8±152.6	0.085
70 keV	−521.6±107.4	−546.0±124.7	−494.7±79.2	−454.0±146.8	0.066
80 keV	−530.9±106.3	−555.8±123.1	−503.4±78.4	−464.1±145.0	0.067
90 keV	−540.2±105.1	−565.5±120.9	−512.2±78.2	−472.0±143.7	0.059
100 keV	−547.7±104.5	−573.5±119.1	−519.3±77.9	−478.7±142.2	0.053
110 keV	−553.1±103.3	−579.2±117.9	−524.3±77.6	−483.5±141.1	0.050
120 keV	−556.9±102.8	−583.1±117.0	−527.8±77.5	−486.9±140.4	0.048
130 keV	−559.7±102.5	−586.2±116.4	−530.5±77.4	−489.4±139.9	0.046
140 keV	−562.0±102.2	−588.6±115.9	−532.7±77.3	−491.4±139.4	0.044
Spectral curve					
Slope(k)	2.8±1.0	3.0±1.2	2.6±0.9	2.5±0.9	0.317
Iodine map					
NIC	0.49±0.21	0.51±0.24	0.48±0.18	0.46±0.25	0.629

*, P values for comparison between IA and AIS or MIA. AIS, adenocarcinoma in situ; IA, invasive adenocarcinoma; MIA, minimally IA; TSCT, thin-section computed tomography; CT, computed tomography; HU, Hounsfield unit; GSI, gemstone spectral imaging; slope(k), slope of spectral curve; NIC, normalized iodine concentration; SD, standard deviation.

significant difference between IA and AIS or MIA for the presence of pleural retraction.

There were five limitations in our study. First, this was a retrospective study and the number of patients was relatively small as a result of our strict inclusion criteria, especially the cases of IA, and additionally, the cases of AAH were deleted because of the small number. The small number of IA might be related to the fact that IA usually presented as mixed GGNs or solid nodules, and less as pGGNs. Our results should be further validated in a prospective manner with a large number of cases, with AAH included too. Second, the sex of cases in our study was quite unbalanced, the possible reason would be the higher incidence rate of lung adenocarcinoma in female. And more male patients should be included in the future study. Third, we included only nodules of ≥8 mm in diameter, which may

have contributed to a selection bias. However, pGGNs of <8 mm may rarely represent IA. Third, we did not measure the volume or mass of the lesions. But volumetric measurements might cause error from both human and computer, and it remains an issue for small GGNs (1). And when we measured diameters of the target lesions, we made multiple planar reconstruction and measured the maximum diameter. Forth, CT number was measured from different CT scans, including CT number acquired from unenhanced TSCT imaging and serials of enhanced monochromatic spectral imaging at a 10-keV interval from 40 to 140 keV. However, our purpose was to investigate the value of both monochromatic imaging and iodine map to differentiate pGGNs, and enhancement was needed. Unenhanced monochromatic imaging was not included in our study for the reason of avoiding extra exposure. In future, we

Table 5 Correlation between imaging parameters and pathology

Parameters	r	P values
Bubble lucency	0.099	0.471
Lobulation	0.083	0.545
Pleura retraction	0.332	0.013
Bronchi in pGGNs	−0.220	0.106
Vessels in pGGNs	0.264	0.051
Size	0.303	0.024
Nonenhanced CT number	0.179	0.192
Enhanced monochromatic imaging		
40 keV	0.098	0.478
50 keV	0.118	0.390
60 keV	0.175	0.202
70 keV	0.183	0.182
80 keV	0.180	0.188
90 keV	0.193	0.158
100 keV	0.193	0.158
110 keV	0.190	0.164
120 keV	0.201	0.142
130 keV	0.206	0.132
140keV	0.208	0.127
Slope(k)	−0.198	0.147
NIC	−0.121	0.379

pGGN, pure ground-glass nodule; CT, computed tomography; slope(k), slope of spectral curve; NIC, normalized iodine concentration.
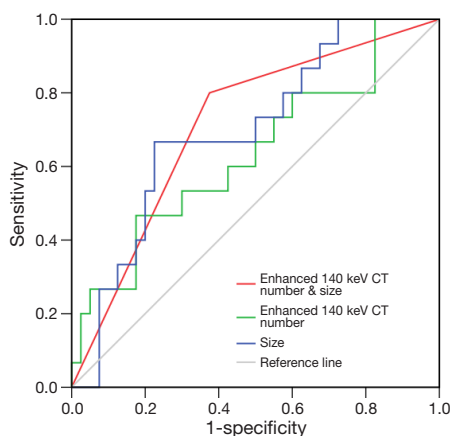

Figure 5 ROC curves for indicating invasive adenocarcinoma. ROC, receiver operating characteristic; CT, computed tomography.

could analyze the value of CT number of unenhanced monochromatic imaging for GGNs differentiation. Fifth, test of quantifying microvessel densities was not included in our study. Since our study is a retrospective study, and this test is not easy to be carried out in our institution. In future, a prospective study including test of quantifying microvessel densities is needed.

Conclusions

DECT could help demonstrate blood supply and indicate the invasion extent of pGGNs, and monochromatic CT number of higher energy (especially 140 keV) would be better for diagnosing IA than lower energies. Together with the size of pGGNs, the diagnostic capacity of IA could be better.

Acknowledgements

Footnote

Conflicts of Interest: The authors have no conflicts of interest to declare.

Ethical Statement: This research was approved by the Institutional Ethics Board of Renji Hospital, School of Medicine, Shanghai Jiaotong University (No. 2017-082). Written informed consent for the use of CT scanning information was obtained from each patient.

References

1. Travis WD, Brambilla E, Noguchi M, et al. International Association for the Study of Lung Cancer/American Thoracic Society/European Respiratory Society International Multidisciplinary Classification of Lung Adenocarcinoma. J Thorac Oncol 2011;6:244-85.
2. Travis WD, Brambilla E, Nicholson AG, et al. The 2015 World Health Organization Classification of Lung Tumors: Impact of Genetic, Clinical and Radiologic

Advances Since the 2004 Classification. J Thorac Oncol 2015;10:1243-60.

3. Van Schil PE, Asamura H, Rusch VW, et al. Surgical implications of the new IASLC/ATS/ERS adenocarcinoma classification. Eur Respir J 2012;39:478-86.

4. Son JY, Lee HY, Lee KS, et al. Quantitative CT analysis of pulmonary ground-glass opacity nodules for the distinction of invasive adenocarcinoma from pre-invasive or minimally invasive adenocarcinoma. PLoS One 2014;9:e104066.

5. Lim HJ, Ahn S, Lee KS, et al. Persistent pure ground-glass opacity lung nodules ≥10 mm in diameter at CT scan: histopathologic comparisons and prognostic implications. Chest 2013;144:1291-9.

6. Si MJ, Tao XF, Du GY, et al. Thin-section computed tomography– histopathologic comparisons of pulmonary focal interstitial fibrosis, atypical adenomatous hyperplasia, adenocarcinoma in situ, and minimally invasive adenocarcinoma with pure ground-glass opacity. Eur J Radiol 2016;85:1708-15.

7. Moon Y, Sung SW, Lee KY, et al. Pure ground-glass opacity on chest computed tomography: predictive factors for invasive adenocarcinoma. J Thorac Dis 2016;8:1561-70.

8. Jin X, Zhao SH, Gao J, et al. CT characteristics and pathological implications of early stage (T1N0M0) lung adenocarcinoma with pure ground-glass opacity. Eur Radiol 2015;25:2532-40.

9. Ko JP, Suh J, Ibidapo O, et al. Lung Adenocarcinoma: Correlation of Quantitative CT Findings with Pathologic Findings. Radiology 2016;280:931-9.

10. Lee HJ, Goo JM, Lee CH, et al. Predictive CT findings of malignancy in ground-glass nodules on thin-section chest CT: the effects on radiologist performance. Eur Radiol 2009;19:552-60.

11. Lee HY, Choi YL, Lee KS, et al. Pure ground-glass opacity neoplastic lung nodules: histopathology, imaging, and management. AJR Am J Roentgenol 2014;202:W224-33.

12. Ikeda K, Awai K, Mori T, et al. Differential diagnosis of ground-glass opacity nodules: CT number analysis by three-dimensional computerized quantification. Chest 2007;132:984-90.

13. Li M, Gao F, Jagadeesan J, et al. Incremental value of contrast enhanced computed tomography on diagnostic accuracy in evaluation of small pulmonary ground glass nodules. J Thorac Dis 2015;7:1606-15.

14. Aoki M, Takai Y, Narita Y, et al. Correlation between tumor size and blood volume in lung tumors: a prospective study on dual-energy gemstone spectral CT imaging. J

Radiat Res 2014;55:917-23.

15. Kawai T, Shibamoto Y, Hara M, et al. Can dual-energy CT evaluate contrast enhancement of ground-glass attenuation? Phantom and preliminary clinical studies. Acad Radiol 2011;18:682-9.

16. Son JY, Lee HY, Kim JH, et al. Quantitative CT analysis of pulmonary ground-glass opacity nodules for distinguishing invasive adenocarcinoma from non-invasive or minimally invasive adenocarcinoma: the added value of using iodine mapping. Eur Radiol 2016;26:43-54.

17. De Cecco CN, Darnell A, Rengo M, et al. Dual-energy CT: oncologic applications. AJR Am J Roentgenol 2012;199:S98-105.

18. Johnson TR, Krauss B, Sedlmair M, et al. Material differentiation by dual energy CT: initial experience. Eur Radiol 2007;17:1510-7.

19. Chae EJ, Song JW, Krauss B, et al. Dual-energy computed tomography characterization of solitary pulmonary nodules. J Thorac Imaging 2010;25:301-10.

20. Zhang M, Kono M. Solitary pulmonary nodules: evaluation of blood flow patterns with dynamic CT. Radiology 1997;205:471-8.

21. Zhang Y, Cheng J, Hua X, et al. Can Spectral CT Imaging Improve the Differentiation between Malignant and Benign Solitary Pulmonary Nodules? PLoS One 2016;11:e0147537.

22. Silva AC, Morse BG, Hara AK, et al. Dual-energy (spectral) CT: applications in abdominal imaging. Radiographics 2011;31:1031-46.

23. Lee SM, Park CM, Goo JM, et al. Invasive pulmonary adenocarcinomas versus preinvasive lesions appearing as ground-glass nodules: differentiation by using CT features. Radiology 2013;268:265-73.

24. Oda S, Awai K, Liu D, et al. Ground-glass opacities on thin-section helical CT: differentiation between bronchioloalveolar carcinoma and atypical adenomatous hyperplasia. AJR Am J Roentgenol 2008;190:1363-8.

25. Kim HY, Shim YM, Lee KS, et al. Persistent pulmonary nodular ground-glass opacity at thin-section CT: histopathologic comparisons. Radiology 2007;245:267-75.